Microchimica Acta (2021) 188: 119
https://doi.org/10.1007/s00604-021-04775-4

ORIGINAL PAPER

Functionalized ultra-fine bimetallic PtRu alloy nanoparticle with high peroxidase-mimicking activity for rapid and sensitive colorimetric quantification of C-reactive protein

Pramod K. Gupta[1] · Seong Eun Son[1] · Gi Hun Seong[1]

Received: 3 October 2020 / Accepted: 22 February 2021 / Published online: 9 March 2021

Abstract

The in situ synthesis is reported of citric acid-functionalized ultra-fine bimetallic PtRu alloy nanoparticles (CA@PtRu ANPs) through a simple one-pot wet chemical method. The cost-efficient CA@PtRu ANPs with an average diameter of 3.2 nm revealed to have enhanced surface area, peroxidase-like activity, high stability, and adequate availability of functional groups to bind biomolecules. Along with nanoparticle surface area, the surface charge has also significantly affected the peroxidase-like activity and the colloidal suspension stability. As an excellent immobilization matrix and peroxidase mimic, the CA@PtRu ANPs were utilized to develop non-enzymatic colorimetric immunoassay for rapid, selective, and sensitive quantification of C-reactive protein (CRP) biomarkers. In this immunoassay, CA@PtRu ANPs serve as enzyme mimic that significantly amplifies the color signals, and amine-functionalized silica-coated magnetic microbeads (APTES/SiO_2@Fe_3O_4) act as CRP-recognizing capture probes. The absorbance curves of colorimetric immunoassay were measured in wavelengths between 550 and 750 nm, and the maximum absorbance at 652 nm was used to establish a linear relationship between absorbance and CRP concentrations. The developed colorimetric immunoassay showed rapid and sensitive quantification of CRP levels from 0.01 to 180 μg mL^{-1} with a LOD of 0.01 μg mL^{-1}. Moreover, the mean recovery of CRP from spiked human serum samples lies between 97 and 109% (n = 3), which indicates that the proposed nanozyme-linked immunoassay has the potential to be used in rapid point-of-care applications.

Keywords Bimetallic alloy · Nanozyme · Immunoassay · C-reactive protein · Colorimetric detection

Introduction

To date, a variety of nanomaterials, especially metal nanoparticles, have been recognized to possess intrinsic enzyme-like activity (nanozymes) [1]. In particular, Pt is considered a promising nanozyme for biomedical applications due to its excellent stability, catalytic activity, and surface properties [2]. Even though Pt nanostructures are dynamic nanozymes, their constrained worldwide availability and high cost limit their bulk use and the commercialization of Pt-based applications. The use of Pt-based bimetallic alloy nanoparticles as exceptionally efficient nanozymes is one of the unique alternatives to Pt nanostructures that can resolve the issues related to utilization cost and commercialization [3]. Pt-based bimetallic surfaces are highly fascinating due to the bifunctional mechanism and synergistic effect between the underlying metals, which often provides enhanced stability and activity compared to monometallic nanostructures [4]. Among the explored Pt-based bimetallic catalysts, PtRu alloy nanoparticles have proven to be the most viable catalysts for methanol oxidation and fuel cell applications [5]. Moreover, Ru nanoparticles possess intrinsic peroxidase-like activity, and it is one of the promising metals to alloy with Pt because the expanded capacity of the bimetallic PtRu alloy surface enhances the oxidation process [6]. Although PtRu has incredible potential for enzyme-like activity, only a few studies have explored PtRu alloy nanoparticle's application as efficient nanozymes to develop practical biosensing applications.

Early detection of diseases can increase the likelihood of successful treatment by improving therapeutic decision-making. C-reactive protein (CRP) is an important biomarker of

✉ Gi Hun Seong
ghseong@hanyang.ac.kr

[1] Department of Bionano Engineering, Center for Bionano Intelligence Education and Research, Hanyang University, Ansan 426-791, South Korea

inflammation and infections, which produced in the liver and found in human blood plasma [7]. An abnormal level of CRP in human blood is directly linked to several diseases, including hypertension, diabetes, cardiovascular diseases, and viral and bacterial infections [8–11]. Thus an elevated level of CRP in patients is a significant factor in the diagnosis of these lethal diseases. Conventional detection methods, including clinical immunoassay, fluorescence immunoassay, vertical flow immunoassay, electrochemical immunoassay, lateral flow immunoassay, chemiluminescence immunoassay, and chromatographic sensors, are not sensitive enough for quantification of a wide range of CRP levels [12, 13]. Moreover, these techniques are more time-consuming, costly, nontransferable, and/or require human expertise, all of which obstructs implementation in large-scale disease screening. Therefore, it is essential to develop alternative approaches for facile, fast, sensitive, and selective CRP quantification in a wide linear range for routine health screening.

Recently, novel colorimetric sensors have attracted massive attention in biosensing applications due to their simple design and high sensitivity [14–17]. Of these applications, the enzyme-linked immunoassay (ELISA) is a well-recognized standard method for quantifying biomarkers in human serum. The critical parameter of this type of biosensing is enzymatic activity. Typically, enzyme-mediated signal amplification strategies employ natural enzymes, such as horseradish peroxidases (HRP), which catalyze the biochemical reactions in the presence of specially designed substrates [18]. Although natural enzymes have high catalytic efficiency, most sensors employing natural enzymes suffer from the limitations of low stability under harsh conditions, loss of activity after modification, high cost, extended preparation time, and difficulty of storage and reuse [19]. The major drawback of traditional ELISA is the required reaction time, which can be 1.5–3 h [20]. The use of nanozymes (artificial enzymes) is an excellent way to overcome the issues with natural enzymes with regard to enzymatic signal amplification [21–23].

To this end, citric acid-functionalized ultra-fine bimetallic PtRu alloy nanoparticles (CA@PtRu ANPs) are proposed as a promising candidate for developing a nanozyme-linked colorimetric immunoassay for rapid and sensitive detection of CRP. The proposed methodology's success lies in the controlled synthesis of nanoscale bimetallic particles with a high surface-to-volume ratio with the desired composition. Therefore, CA@PtRu ANPs were synthesized using a one-pot wet chemical method that offers the advantages of simultaneous reduction of the two metal precursors, facile synthesis, and control of particle size [24]. The composition of Pt and Ru metal precursors for synthesizing CA@PtRu ANPs was kept to a 1:1 ratio to utilize the full potential of the alloy nanostructures. In the proposed immunoassay, the use of magnetic beads offered an easy and fast way to separate the immunocomplex. Accuracy of immunoassay was examined for the detection of CRP in human serum samples. The obtained result suggests that the utilization of a nanozyme in place of a natural enzyme is an excellent choice for the clinical quantification of CRP.

Materials and methods

Synthesis of PtRu and CA@PtRu ANPs

Detailed reagents information is provided in the Supplementary Information (SI). To synthesize the CA@PtRu ANPs, 1 mM H_2PtCl_6 and 1 mM $RuCl_3.xH_2O$ were dissolved in 40 mL of deionized water. Electrostatic interaction occurs between the negatively charged $PtCl_6$ ions and the positively charged Ru ions in the aqueous medium. A separate aqueous solution of 8 mM $C_6H_8O_7$ (10 mL) was prepared and added dropwise with the Pt/Ru solution under continuous stirring; stirring was continued for 1 h for homogeneous mixing. Next, a freshly prepared 50 mM $NaBH_4$ in ice-cold deionized water (10 mL) was slowly added to the $H_2PtCl_6 + RuCl_3.xH_2O + C_6H_8O_7$ solution under continuous stirring at room temperature. The addition of $NaBH_4$ leads to the simultaneous reduction of the Pt and Ru precursors in the presence of citric acid, and the nucleation process gives rise to the formation of well-dispersed alloy nanoparticles. After 3 h of continuous stirring, the obtained product was placed into dialysis tubing that was then closed off at both ends and transferred into a beaker containing 5 L of water. The surrounding water was changed every 8 h over 2 days to neutralize pH and remove impurities. The dialyzed alloy nanoparticles were re-dispersed in deionized water and stored at room temperature. A schematic of the synthesis of CA@PtRu ANPs is shown in Scheme S1. For comparison, Ru, Pt, and PtRu alloy NPs were also prepared using similar methods, except for the use of $C_6H_8O_7$.

Preparation of detection probe (dAb-CRP/CA@PtRu ANPs)

Prior to the conjugation process, the CA@PtRu ANPs were treated with 1-ethyl-3-(3-dimethylaminopropyl)carbodiimide and N-hydroxysuccinimide (EDC-NHS) to activate the carboxyl groups present on their surfaces. First, 0.4 mM EDC and 0.4 mM NHS were dispersed in 1.5 mL MES buffer (0.1 M, pH 6) containing 200 μg CA@PtRu ANPs and incubated for 1.5 h at room temperature. The EDC-NHS-activated CA@PtRu ANPs were then washed with PBS to remove excess EDC-NHS and re-dispersed in PBS (0.1 M, pH 7.4). EDC-NHS-activated CA@PtRu ANPs were introduced to different concentrations of dAb-CRP with weight ratios of 1:2.5, 1:1.6, 1:1, and 1:0.8. An optimal amount of activated CA@PtRu ANPs (200 μg) and dAb-CRP (165 μg) in PBS

(0.1 M, pH 7.4) were mixed in an Eppendorf tube, followed by incubation on a shaker for 6 h. During this time, dAb-CRP covalently attached to the CA@PtRu ANPs to serve as a detection probe. Subsequently, dAb-CRP/CA@PtRu conjugates were washed with PBS to discard unattached dAb-CRP, and the conjugates were re-dispersed in 1.1 mL of PBS. The dAb-CRP/CA@PtRu conjugates were stored at 4 °C until further use.

Preparation of standard and spiked CRP concentrations

Different concentrations of CRP ranging from 0.01 to 180 μg mL^{-1} were prepared in 0.1 M PBS containing 25% fetal bovine serum. In the case of spiked serum samples, different CRP concentrations (0.01, 6.25, and 90 μg mL^{-1}) were set up by adding CRP antigen in undiluted CRP free serum. Detailed information regarding the procedures to prepare APTES/SiO_2@Fe_3O_4 magnetic microbeads, capture probe (cAb-CRP/APTES/SiO_2@Fe_3O_4), evaluate the enzyme-like activity, and use characterization techniques are provided in the SI.

Detection of CRP

Each 100 μL of the prepared capture probe (cAb-CRP/APTES/SiO_2@Fe_3O_4) was placed in different Eppendorf tubes, and each tube was separately introduced to 50 μL of varying concentrations of CRP from 0.01 to 180 μg mL^{-1}. These tubes were incubated overnight (8 h) on a vertical rotator at 10–15 °C to form CRP/cAb-CRP/APTES/SiO_2@Fe_3O_4 immunocomplexes. The resultant immunocomplexes were washed with PBS and magnetically separated to remove unattached CRP. The immunocomplex (CRP/cAb-CRP/APTES/SiO_2@Fe_3O_4) produced for various concentrations of CRP (0.01–180 μg mL^{-1}) was separately mixed with the 100 μL of dAb-CRP/CA@PtRu conjugates (detection probes) and incubated for 1 h on a vertical rotator at room temperature. The resulting sandwich-like immunocomplexes were washed three times with PBS, followed by magnetic separation to collect only sandwich-like structures while discarding others. Subsequently, 800 μL of pH 4 phthalate buffer, 100 μL of TMB (5 mM) in ethanol, and 100 μL of H_2O_2 (100 mM) were separately added to the sandwich-like immunocomplex solution at each CRP concentration and incubated for 2 min at room temperature. At this point, the immunocomplex was separated by applying a magnetic field, and the supernatant (blue colored product) was transferred to cuvette to record the absorbance in the range of 550 to 750 nm. The absorbance peak at a wavelength of 652 nm was used to establish calibration plot between absorbance and CRP concentrations. The unknown CRP concentration (unknown sample) can also be detected using above protocol.

Results and discussions

Working principle of immunoassay for CRP detection

The fundamental idea behind the developed nanozyme-linked immunoassay for sensitive, selective, and rapid CRP quantification is displayed in Scheme 1. The proposed method relies on a monoclonal capture antibody specific to CRP (cAb-CRP) immobilized on APTES/SiO_2@Fe_3O_4 magnetic microbeads to serve as the capture probe and CA@PtRu ANPs (nanozyme) linked to a detection antibody (dAb-CRP) to serve as the detection probe. The detection probe is prepared by covalent attachment of dAb-CRP with EDC-NHS-activated CA@PtRu ANPs [Scheme 1 (a)]. On the other hand, APTES/SiO_2@Fe_3O_4 microbeads exhibiting the desired functional groups were used as a platform for covalent immobilization of cAb-CRP, which serve to recognize CRP via specific antibody-antigen interaction [Scheme 1 (b)]. In addition, the surface of the capture probe was passivated with BSA to block unspecific sites. Finally, the combination of dAb-CRP/CA@PtRu ANPs (detection probe) and CRP/cAb-CRP/APTES/SiO_2@Fe_3O_4 (capture probe) form a sandwich-like structure via the immunoreaction between CRP (antigen) and dAb-CRP (antibody) [Scheme 1 (c)]. Magnetic separation was performed to collect only the sandwich-like immunocomplex and discard the others, including excess dAb-CRP-CA@PtRu ANPs. The absence of CRP prevents the formation of the sandwich-like immunocomplex, i.e., there is a lack of CA@PtRu ANPs in the magnetically separated sample. Furthermore, the concentration of the sandwich-like immunocomplex varies with the amount of CRP attached to the capture probe. The CA@PtRu ANPs present in the sandwich-like immunocomplex catalyzes the oxidation of the TMB substrate in the presence of H_2O_2, which produces the colorimetric signal [21]. In this way, the colorimetric signal intensity is directly proportional to the concentration of CRP.

Characterization of CA@PtRu ANPs

The crystallinity of the as-synthesized Ru NPs, Pt NPs, PtRu ANPs, and CA@PtRu ANPs was studied using XRD, as shown in Fig. S1. Diffraction spectra of Ru and Pt reveal typical peaks related to the hexagonal close-packed (hcp) structure of metallic Ru (JCPDS 01-077-3315) and the face-centered cubic (fcc) structure of metallic Pt (JCPDS 01-087-0640), respectively. In the case of PtRu, a shift in the diffraction peak positions of the (111), (200), and (220) planes to higher 2θ were observed, which suggests the incorporation of Ru in the Pt lattice [25]. In addition, the absence of distinct peaks related to Ru, Pt, or their oxides in the PtRu ANPs diffractogram suggests the alloying of Ru and Pt in fcc structure [26]. The diffractogram of the CA@PtRu ANPs exhibited

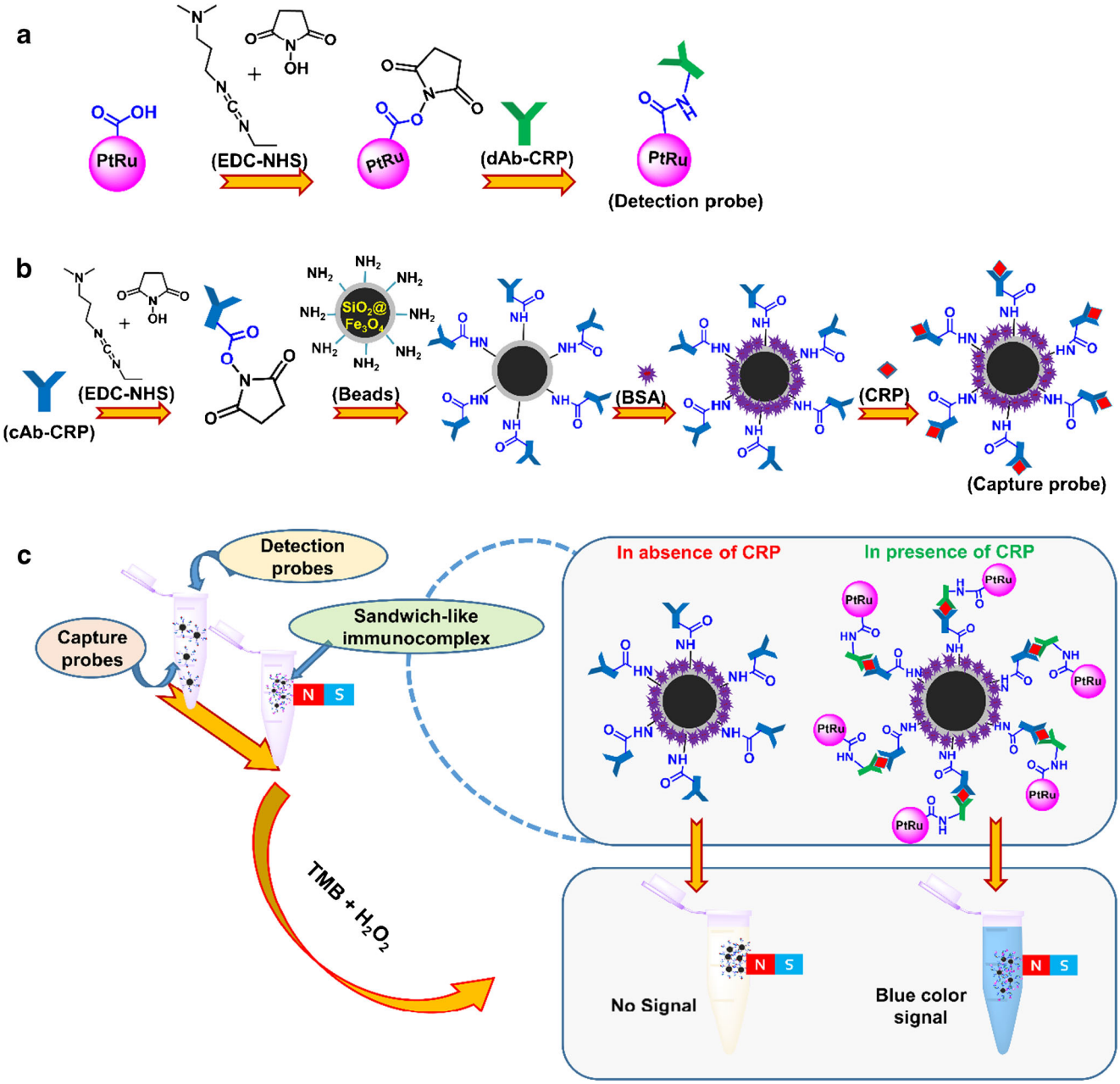

Scheme 1 Schematic of (a) preparation of dAb-CRP/CA@PtRu ANPs conjugates (detection probe), (b) CRP/cAb-CRP/APTES/SiO_2@Fe_3O_4 conjugates (capture probe), and (c) the working methodology for the quantification of CRP

similar peaks as the PtRu ANPs, but with lower intensities, which is indicative of the presence of citric acid on the surface of the PtRu ANPs that reduces reflecting X-rays into the detector [27].

A detailed structural and morphological study of the PtRu and CA@PtRu ANPs was carried out by analyzing their TEM images, as showed in Fig. 1. The image (a) shows nano-agglomerations of ultra-fine PtRu ANPs that are attributed to the heterogeneous interaction between neighboring ANPs. In comparison, image (b) displays well-dispersed ultra-fine CA@PtRu ANPs, as the presence of citric acid on the surface of PtRu ANPs prevents their aggregation. The high-resolution TEM images (c) and (d) show spherically shaped crystalline PtRu and CA@PtRu ANPs, with average particle sizes of 2.5 and 3.2 nm, respectively, as indicated in histograms (e) and (f). The insets of images (c) and (d) show well-defined single PtRu and CA@PtRu ANPs that have a lattice spacing of 0.23 nm, which correspond to the (111) plane of the PtRu alloy structure. The value of the lattice spacing was calculated using Gatan Digital Micrograph® program, and the resulting line profiles of the PtRu and CA@PtRu ANPs are shown in images (g) and (h), respectively. Furthermore, indexing of the

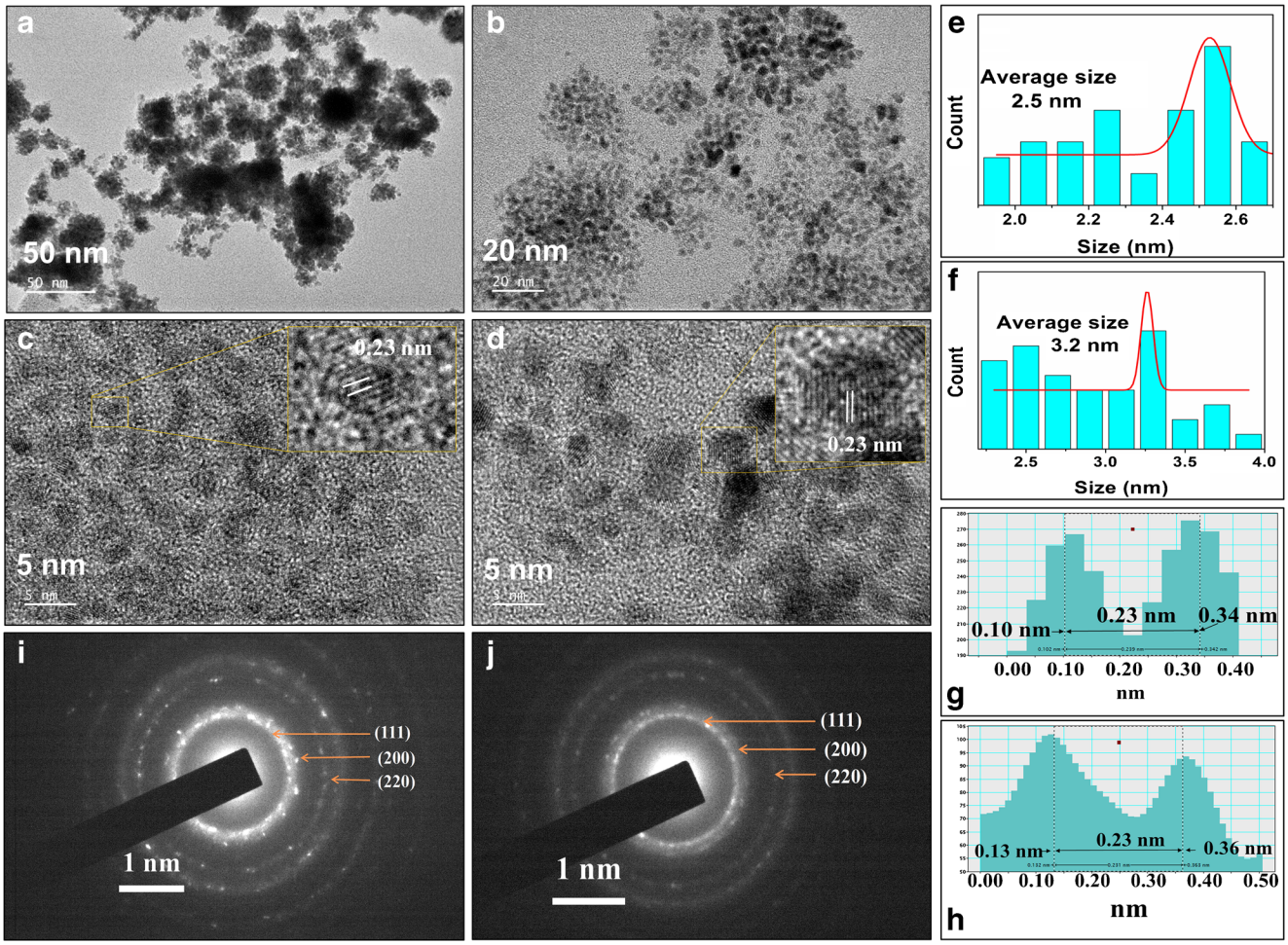

Fig. 1 TEM images (**a**), (**b**); HR-TEM images (**c**), (**d**); histograms for average particle size (**e**), (**f**); line profile for calculating d-spacing (**g**), (**h**); and SAED patterns (**i**), (**j**) for PtRu and CA@PtRu ANPs, respectively

rings in the selected area electron diffraction (SAED) patterns (i) and (j) for PtRu and CA@PtRu ANPs reveals similar planes, (111), (200), and (220), that correspond to the PtRu alloy structure. The TEM results are, therefore, in agreement with XRD analysis.

The XPS investigation of the CA@PtRu ANPs suggests their high purity (Fig. S2). The shift in binding energy for Pt^0 as compared to pure Pt is attributed to the PtRu alloying causing a decrease in the electronic charge density of the platinum atoms, which results in charge transfer between Pt and Ru [28, 29]. The XPS peaks at 284.6, 288.1, and 289 eV correspond to C–C/C=C, C=O, and COOH groups, confirming the presence of citric acid in CA@PtRu ANPs [30]. The elemental ratio of Pt and Ru was calculated to be 46.33%:53.66%, which is nearly equal to the ratio of their precursors (50%:50%) in the synthesis solution. The detailed XPS investigation is discussed in SI. In addition, EDAX mapping displays a uniform distribution of (b) C, (c) Ru, and (d) Pt, (e) O, and (f) combination of C-Ru-Pt-O, within a particular area (a) on the CA@PtRu ANPs (Fig. S3).

The relatively high value of zeta potential for CA@PtRu ANPs (−37.4 mV) suggests that their excellent dispersibility in an aqueous medium is due to the high electrostatic repulsion between the carboxylic groups linked PtRu ANPs, as detailed in the SI (Fig. S4). In addition to increasing colloidal stability, the high negative charge of the ANPs attracts TMB substrate and binds closer to the PtRu ANPs surface, which enhances the electron transfer rate and, thus, oxidation of the substrate.

Characterization of magnetic microbeads

The Fe_3O_4 microparticles were covered with silica (SiO_2) to suppress their enzyme-like activity and provide high stability. The SiO_2@Fe_3O_4 particles were further functionalized with (3-aminopropyl)-triethoxysilane (APTES) to ensure adequate functional groups for covalent immobilization of cAb-CRP. The successful formation of APTES/SiO_2@Fe_3O_4 magnetic beads was validated using EDAX and zeta potential measurements. Compared to EDAX spectra of bare Fe_3O_4 particles,

spectra of APTES/SiO_2@Fe_3O_4 particles reveal enhanced silicon and oxygen content and a decrease in iron (Fe) composition, which suggests the presence of a SiO_2 layer on the surface of the Fe_3O_4 particles (Fig. S5). In addition, the presence of nitrogen and the high carbon content in the EDAX of APTES/SiO_2@Fe_3O_4 indicates the presence of APTES, as detailed in the SI. A sequential change in the zeta potential from Fe_3O_4 (−9.5 mV) to SiO_2@Fe_3O_4 (−22 mV) to APTES/SiO_2@Fe_3O_4 (19 mV) also indicates a successful modification of Fe_3O_4 with silica and APTES, as shown in the SI (Fig. S6). FTIR was carried out at every step of the capture probe (BSA/cAb-CRP/APTES/SiO_2@Fe_3O_4) preparation further to validate the successful modification of the Fe_3O_4 particles, as shown in Fig. S7. FTIR studies also confirm covalent binding between activated carboxylic groups of cAb-CRP and the amine groups of the APTES/SiO_2@Fe_3O_4 particles, as detailed in the SI. A control study confirms that APTES/SiO_2/Fe_3O_4 does not show activity towards the oxidation of the TMB substrate in the presence of H_2O_2 (Fig. S8). Compared to the bare Fe_3O_4 (83.6 amu/g), the lower magnetic saturation (M_s) value for APTES/SiO_2@Fe_3O_4 (78.8 amu/g) was due to the nonmagnetic layer of APTES/SiO_2 over magnetic Fe_3O_4 particles. However, APTES/SiO_2@Fe_3O_4 microbead particles have retained a strong magnetization for magnetic separation, detailed in SI (Fig. S9a). Furthermore, the optimized time for magnetic separation was determined by observing the change in absorption of the aqueous APTES/SiO_2@Fe_3O_4 solution for the time of the magnetic field applied and found to be 30 s Fig. S9b).

Enzyme-like activity of PtRu and CA@PtRu ANPs

Figure S10a clearly shows that the introduction of Ru NPs, Pt NPs, PtRu ANPs, and CA@PtRu ANPs converts the colorless TMB + H_2O_2 solution into a dark blue colored product (oxidized TMB, TMB_{ox}) [21]. The light blue color in the absence of H_2O_2 indicates the weak oxidase-like activity of PtRu and CA@PtRu ANPs. Both Ru and Pt NPs have good intrinsic peroxidase-like activity (Fig. S10b). A decrease in peroxidase-like activity is observed for PtRu ANPs due to the aggregation of ANPs, as indicated by TEM results. This issue of aggregation is resolved by the in situ functionalization of PtRu ANPs with citric acid. The well-dispersed ultra-fine CA@PtRu ANPs exhibit high surface area, negatively charged surfaces, and oxygenated functional groups that produce high peroxidase-like activity (Fig. S10b). Figure S10c reveals weak oxidase-like activity of PtRu and CA@PtRu ANPs, which can be ignored compared to their peroxide-like activity. These findings suggest that the peroxidase-like activity of the as-synthesized nanomaterials critically depends on their surface area and surface charge.

In the case of the PtRu ANPs, maximum peroxidase-like activity was observed at pH 4, while that of the CA@PtRu ANPs was at pH 5 (Fig. S10d). In addition, PtRu and CA@PtRu ANPs revealed maximum peroxidase-like activity at 50 and 60 °C, respectively (Fig. S10e). Figure S10f reveals that the peroxidase-like activity of PtRu and CA@PtRu ANPs increases with their concentrations. Moreover, CA@PtRu ANPs retain higher peroxidase-like activity than PtRu ANPs even after 1 month of storage in aqueous solution at room temperature (Fig. S10g). The detailed optimizations are discussed in SI.

The kinetic parameters, maximal reaction velocity (V_{max}) and Michaelis constant (K_m), of PtRu ANPs and CA@PtRu ANPs for catalyzing oxidation of H_2O_2 and TMB substrate were calculated based on Lineweaver–Burk equation, detailed in SI (Figs. S11 and S12). In the case of PtRu ANPs, the values of kinetic parameters K_m and V_{max} for H_2O_2 oxidation were found to be 16.5 mM and 38.9×10^{-8} $Ms.^{-1}$, respectively. In contrast, when H_2O_2 oxidation was performed in the presence of CA@PtRu ANPs, the values of K_m and V_{max} were found to be 14.9 mM and 74.4×10^{-8} $Ms.^{-1}$, respectively. Under similar conditions, the steady-state kinetics for the oxidation of TMB substrate catalyzed by PtRu and CA@PtRu ANPs was studied in the presence of H_2O_2 (Fig. S12). The values of the kinetic parameters K_m and V_{max} for the PtRu ANPs were calculated from the Lineweaver–Burk plot and were found to be 0.016 mM and 4.43×10^{-8} M s^{-1}, whereas, for the CA@PtRu ANPs, the values of K_m and V_{max} were found to be 0.046 mM and 10.19×10^{-8} M s^{-1}, respectively. It is evident that the PtRu ANPs and CA@PtRu ANPs possess higher values of kinetic parameters for H_2O_2 and TMB oxidations as compared to HRP and previously reported nanozymes (detailed discussed in the SI, Table S1).

The surface modification of CA@PtRu ANPs with dAb-CRP results in a decrease in peroxidase-like activity, as shown in Fig. S13a. Interestingly, an increase in activity was observed with an increase in dAb-CRP concentration, but such an increase also induces agglomeration. In addition, dAb-CRP/CA@PtRu ANPs conjugates reveal optimal peroxidase-like activity in a phthalate buffer of pH 4, whereas CA@PtRu ANPs revealed more activity in a pH 5 phthalate buffer (Fig. S13b). The covalent attachment of dAb-CRP on the surface of CA@PtRu ANPs results in a decrease of carboxylic group active sites, which leads to a significant change in the zeta potential (from −37.4 to −19.2 mV) of the dAb-CRP/CA@PtRu ANPs conjugates, as shown in Fig. S13c. Thus, the reason behind the shift of optimum pH can be ascribed to the immobilization of dAb-CRP or change in surface properties of dAb-CRP/CA@PtRu ANPs conjugates.

Detection of C-reactive protein

A CA@PtRu ANPs-based colorimetric immunoassay for quantitative detection of CRP concentrations ranging from 0.01 to 180 μg mL^{-1} was developed using APTES/SiO_2@Fe_3O_4 magnetic microbeads, as previously discussed and illustrated in Scheme 1. Figure 2a shows the optical intensities of the resultant immunocomplex solutions with various concentrations of CRP

after reaction with TMB and H_2O_2. A consecutive increase in blue color intensity was observed for increasing CRP concentration. This change in color intensity was quantified by recording absorption spectra within the wavelength range of 550 to 750 nm, as shown in Fig. 2b. A semilog calibration curve is plotted for the absorbance at 652 nm as a function of corresponding CRP concentration Fig. 2c. The calibration curve shows linear detection of CRP for concentrations ranging from 1.4 to 180 μg mL^{-1} with a LOD of 0.01 μg mL^{-1}. Here, the LOD was estimated based on the lowest intensity of blue color that can be easily detected with the naked eye. The enhanced peroxidase-like activity, i.e., signal amplification ability of the CA@PtRu ANPs, contributes to the high sensitivity and decreased analysis time of the developed colorimetric immunoassay.

The obtained analytical parameters of the proposed CRP quantification method are compared with previously reported biosensing methods in Table 1. The presented colorimetric immunoassay method showed a fast response of 2 min and a broader CRP detection range than previous approaches. The broader detection range of proposed immunoassay can include diagnosis of cardiovascular diseases [8], chronic obstructive pulmonary disease (0.2–11.09 μg mL^{-1}) [9], cerebral small-vessel disease (> 6 μg mL^{-1}) [10], viral infections (10–40 μg mL^{-1}), and bacterial infections (>40 μg mL^{-1}) [11]. The LOD of the proposed immunoassay is also under the low-risk limit value (1 μg mL^{-1}) set by the American Heart Association and the Centers for Disease Control and Prevention (AHA/CDC). The simplicity, stability, sensitivity, and cost-efficiency of CA@PtRu ANPs-based colorimetric immunoassays make it highly suitable for rapid point-of-care applications.

The selectivity of the developed immunoassay for CRP detection was examined in the presence of potential interferents such as ascorbic acid, urea, glucose, human serum albumin (HSA), and creatinine. The high affinity of monoclonal CRP antibodies (dAb-CRP and cAb-CRP) to CRP antigen enables the high selectivity to the immunoassay, detailed in SI (Fig. S14). The accuracy of the proposed nanozyme-linked immunoassay to be used in point-of-care applications was examined by measuring three different CRP concentrations in spiked human serum samples (0.01, 6.25, and 90.0 μg mL^{-1}). It was found that the proposed immunoassay is able to recover 97–109% of CRP from spiked human serum samples with the RSD value of 3.8–4.7% (Table 2). These values of recovery are in an acceptable range.

Conclusions

A colorimetric immunoassay based on in situ functionalized, ultra-fine, bimetallic CA@PtRu ANPs has been developed for rapid, selective and sensitive quantification of CRP. CA@PtRu ANPs, synthesized by a simple one-pot wet chemical method, show a high surface area, significant negative surface charge, enhanced nanozyme activity, high stability to harsh surrounding conditions, and adequate functional groups for covalent attachment of biomolecules. Nanoparticle surface

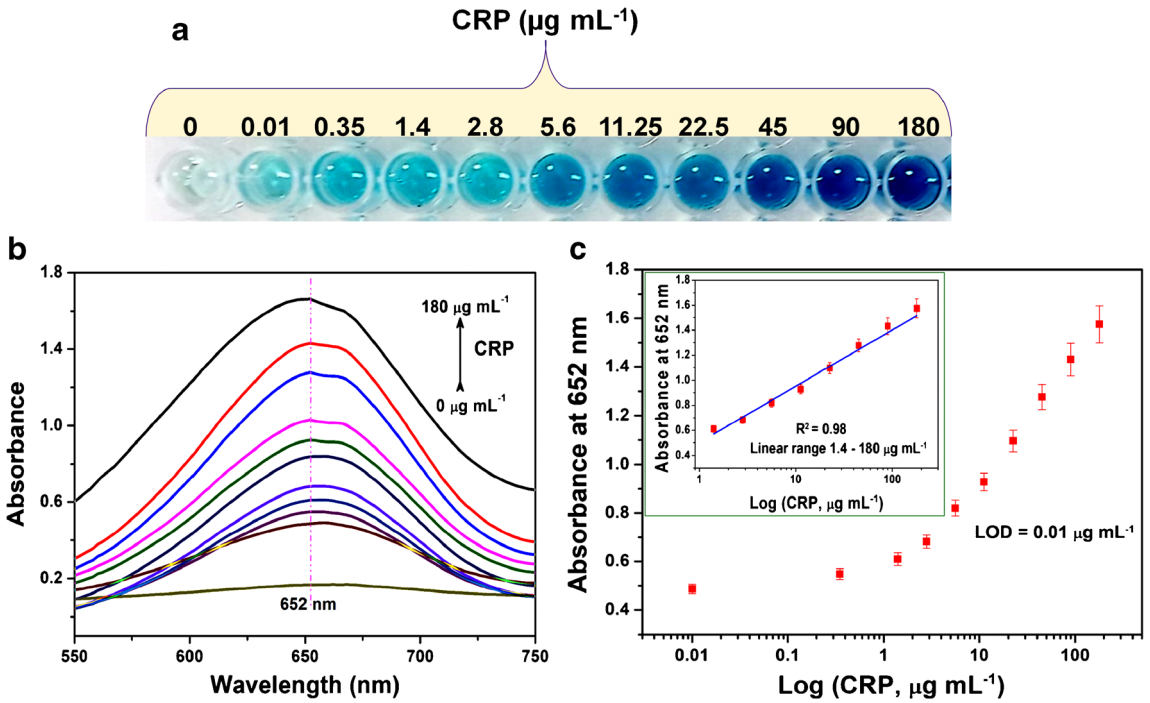

Fig. 2 **a** Optical intensity and **b** absorbance spectra of the resultant immunocomplex solution for various concentrations of CRP (0.01 to 180 μg mL^{-1}) after reaction with TMB and H_2O_2. **c** Semilog calibration curve of the absorbance intensities at 652 nm as a function of CRP concentration

Table 1 Overview of recently reported nanomaterial-based analytical methods for the CRP determination with the proposed CA@PtRu ANPs-based colorimetric immunoassay

Materials used	Detection technique	Detection range (μg mL^{-1})	Detection limit (μg mL^{-1})	Reaction/ response time	Total assay time (≥)	Ref.
Droplet microfluidic + MB	Fluorescence	0.01–0.05	0.01	60 min	60 min	[31]
Combination of FCF, FTH, and ASPM	VFA	0.01–10	0.01	2 min	2 min	[32]
3D paper	VFA	0.005–5	0.005	15 min	15 min	[33]
Aptamer-MB/SPCE	Electrochemical	0.1–50	0.054	5 min	45 min	[34]
rGO/Ni/PtNPs micromotors	Electrochemical	2–100	0.08	5 min	7 min	[35]
MoS_2–PANI–AuNPs	Electrochemical	0.0002–0.08	0.0002	50 min	50 min	[36]
Au electrodes	Electrochemical	0.055–5.5	0.021	30 min	30 min	[37]
Carbon nanofiber	Electrochemical	0.05–5	0.011	60 min	75 min	[38]
Au(MPA)-PPy/ITO electrode	Electrochemical	0.01–10	0.019	30 min	30 min	[39]
Ir NPs/GO-DN	Electrochemical	0.00001–0.1	3.3×10^{-6}	60 min	105 min	[40]
Diamond	Electrochemical	1.1–110	1.1	60 min	180 min	[41]
CdSe/ZnS QDs	LFA	0.025–1.6	0.0039	20 min	20 min	[42]
MOF	ECL	0.001–0.4	0.0002	60 min	60 min	[43]
Au NPs	Chromatographic	1–15	0.6	15 min	135 min	[20]
MB	Micro-MEMS-fluxgate sensor	0.002–10	0.002	5 s	30 min	[12]
Pt-RTD	Photothermal	0.0001–0.1	0.0001	90 s	60 min	[44]
NRD	ATR-FTIR	10–20	10	90 min	90 min	[45]
Aptamer-AuNPs	Colorimetric	0.0001–0.2	8×10^{-6}	15 min	77 min	[46]
Ag NPs	Colorimetric	0.0015–0.025	0.001	20 min	45 min	[47]
NB-rGO sheets	Colorimetric	0.001–5	0.005	3 min	240 min	[48]
Citrate-capped Au NPs	Colorimetric	0.889–20.7	1.2	5 min	5 min	[14]
CA@PtRu ANPs	Colorimetric	0.01–180	0.01	2 min	542 min	Present work

ATR-FTIR attenuated total reflection Fourier transform infrared; *ASPM* asymmetric membrane; *ECL* electrochemiluminescence; *FCF* flow control film; *FTH* flow-through holes; *ITO* indium tin oxide; *LFA* lateral flow assay; *LMR* lossy mode resonances; *MB* magnetic beads; *MEMS* microelectromechanical system; *MOF* metal-organic framework; *MPA* 3-mercaptopropionic acid; *NPs* nanoparticles; *NRD* nanocrystalline diamond; *PANI* polyaniline; *PPy* polypyrrole; *Pt-RTD* platinum resistive temperature detector; *QDs* quantum dots; *SERRS* surface-enhanced resonance Raman scattering; *SPCE* screen-printed carbon electrode; *VFA* vertical flow immunoassay

area was observed to have a higher impact on enzyme-like activity than did surface charge. Covalent immobilization of antibodies (cAb-CRP and dAb-CRP) towards the fabrication of capture and detection probes provides high stability to the proposed method. The use of magnetic particles as beads (APTES/SiO_2@Fe_3O_4) offers a quick and straightforward approach to isolate the immunocomplex. The proposed immunoassay revealed rapid detection at a wide range of CRP concentrations, enabling risk prediction for a host of lethal diseases, including cardiovascular diseases, chronic obstructive pulmonary disease, cerebral small-vessel disease, viral infections, and bacterial infections. In addition, negligible interactions with interference molecules and good recovery of CRP from the spiked human serum sample validate the high accuracy of demonstrated immunoassay. The principles behind the developed immunoassay can also be applied to the detection of numerous other biomarkers as well.

Table 2 Recovery of CRP from spiked human serum samples as determined by CA@PtRu ANPs-linked immunoassay

CRP in undiluted human serum (μg mL^{-1})	Added CRP level (μg mL^{-1})	CRP in spiked human serum sample (μg mL^{-1})	Found (μg mL^{-1})	Mean recovery (n =3)	RSD (%)
0.02	0.01	0.03	0.032	106%	4.7
0.02	6.25	6.27	6.08	97%	3.8
0.02	90	90.02	98.1	109%	4.2

Supplementary Information The online version contains supplementary material available at https://doi.org/10.1007/s00604-021-04775-4.

Acknowledgments The authors acknowledge the Ministry of Education for their funding support through Basic Science Research Program under National Research Foundation of Korea (NRF-2018R1A6A1A03024231).

Declarations

Conflict of interest The authors declare no competing interest

References

1. Singh S (2019) Nanomaterials exhibiting enzyme-like properties (nanozymes): current advances and future perspectives. Front Chem 7:46
2. Jeyaraj M, Gurunathan S, Qasim M et al (2019) A comprehensive review on the synthesis, characterization, and biomedical application of platinum nanoparticles. Nanomater (Basel, Switzerland) 9: 1719. https://doi.org/10.3390/nano9121719
3. Song W, Zhao B, Wang C, Ozaki Y, Lu X (2019) Functional nanomaterials with unique enzyme-like characteristics for sensing applications. J Mater Chem B 7:850–875. https://doi.org/10.1039/C8TB02878H
4. Cai S, Qi C, Li Y, Han Q, Yang R, Wang C (2016) PtCo bimetallic nanoparticles with high oxidase-like catalytic activity and their applications for magnetic-enhanced colorimetric biosensing. J Mater Chem B 4:1869–1877. https://doi.org/10.1039/C5TB02052B
5. Tian M, Shi S, Shen Y, Yin H (2019) PtRu alloy nanoparticles supported on nanoporous gold as an efficient anode catalyst for direct methanol fuel cell. Electrochim Acta 293:390–398. https://doi.org/10.1016/j.electacta.2018.10.048
6. Bavand R, Korinek A, Botton GA, Yelon A, Sacher E (2017) PtRu alloy nanoparticles I. Physicochemical characterizations of structures formed as a function of the type of deposition and their evolutions on annealing. J Phys Chem C 121:23104–23119. https://doi.org/10.1021/acs.jpcc.7b04434
7. Sproston NR, Ashworth JJ (2018) Role of C-reactive protein at sites of inflammation and infection. Front Immunol 9:754. https://doi.org/10.3389/fimmu.2018.00754
8. Cozlea DL, Farcas DM, Nagy A et al (2013) The impact of C reactive protein on global cardiovascular risk on patients with coronary artery disease. Curr Health Sci J 39:225–231
9. Yanbaeva DG, Dentener MA, Spruit MA, Houwing-Duistermaat JJ, Kotz D, Passos VL, Wouters EFM (2009) IL6 and CRPhaplotypes are associated with COPD risk and systemic inflammation: a case-control study. BMC Med Genet 10:23. https://doi.org/10.1186/1471-2350-10-23
10. Christiane R, Klaus B, P M de Maat M et al (2007) CRP gene haplotypes, serum CRP, and cerebral small-vessel disease. Stroke 38:2356–2359. https://doi.org/10.1161/STROKEAHA.107.482661
11. Zhang P, Bao Y, Draz MS et al (2015) Rapid and quantitative detection of C-reactive protein based on quantum dots and immunofiltration assay. Int J Nanomedicine 10:6161
12. Guo L, Yang Z, Zhi S, Feng Z, Lei C, Zhou Y (2018) A sensitive and innovative detection method for rapid C-reactive proteins analysis based on a micro-fluxgate sensor system. PLoS One 13: e0194631–e0194631. https://doi.org/10.1371/journal.pone.0194631
13. Luo Y, Zhang B, Chen M, Jiang T, Zhou D, Huang J, Fu W (2012) Sensitive and rapid quantification of C-reactive protein using quantum dot-labeled microplate immunoassay. J Transl Med 10: 24. https://doi.org/10.1186/1479-5876-10-24
14. António M, Ferreira R, Vitorino R, Daniel-da-Silva AL (2020) A simple aptamer-based colorimetric assay for rapid detection of C-reactive protein using gold nanoparticles. Talanta 214:120868. https://doi.org/10.1016/j.talanta.2020.120868
15. Yang J, Wang K, Xu H, Yan W, Jin Q, Cui D (2019) Detection platforms for point-of-care testing based on colorimetric, luminescent and magnetic assays: a review. Talanta 202:96–110. https://doi.org/10.1016/j.talanta.2019.04.054
16. Li F, Hu Y, Zhao A et al (2020) β-Cyclodextrin coated porous Pd@au nanostructures with enhanced peroxidase-like activity for colorimetric and paper-based determination of glucose. Microchim Acta 187:425. https://doi.org/10.1007/s00604-020-04410-8
17. Zhao X, Lyu H, Yao X, Xu C, Liu Q, Liu Z, Zhang X, Zhang X (2020) Hydroquinone colorimetric sensing based on platinum deposited on CdS nanorods as peroxidase mimics. Microchim Acta 187:587. https://doi.org/10.1007/s00604-020-04451-z
18. Ronkainen NJ, Halsall HB, Heineman WR (2010) Electrochemical biosensors. Chem Soc Rev 39:1747–1763. https://doi.org/10.1039/B714449K
19. Ju Y, Kim J (2015) Dendrimer-encapsulated Pt nanoparticles with peroxidase-mimetic activity as biocatalytic labels for sensitive colorimetric analyses. Chem Commun 51:13752–13755. https://doi.org/10.1039/C5CC06055A
20. Byzova NA, Zherdev AV, Vengerov YY, Starovoitova TA, Dzantiev BB (2017) A triple immunochromatographic test for simultaneous determination of cardiac troponin I, fatty acid binding protein, and C-reactive protein biomarkers. Microchim Acta 184: 463–471. https://doi.org/10.1007/s00604-016-2022-1
21. Jiang D, Ni D, Rosenkrans ZT, Huang P, Yan X, Cai W (2019) Nanozyme: new horizons for responsive biomedical applications. Chem Soc Rev 48:3683–3704. https://doi.org/10.1039/C8CS00718G
22. Huang Y, Ren J, Qu X (2019) Nanozymes: classification, catalytic mechanisms, activity regulation, and applications. Chem Rev 119: 4357–4412. https://doi.org/10.1021/acs.chemrev.8b00672
23. Wu J, Wang X, Wang Q, Lou Z, Li S, Zhu Y, Qin L, Wei H (2019) Nanomaterials with enzyme-like characteristics (nanozymes): next-generation artificial enzymes (II). Chem Soc Rev 48:1004–1076. https://doi.org/10.1039/C8CS00457A
24. Wei Z, Sun J, Li Y, Datye AK, Wang Y (2012) Bimetallic catalysts for hydrogen generation. Chem Soc Rev 41:7994–8008. https://doi.org/10.1039/C2CS35201J
25. Jiang X, Gür TM, Prinz FB, Bent SF (2010) Sputtered Pt–Ru alloys as catalysts for highly concentrated methanol oxidation. J Electrochem Soc 157:B314. https://doi.org/10.1149/1.3273081
26. Yang X, Zheng J, Zhen M, Meng X, Jiang F, Wang T, Shu C, Jiang L, Wang C (2012) A linear molecule functionalized multi-walled carbon nanotubes with well dispersed PtRu nanoparticles for ethanol electro-oxidation. Appl Catal B Environ 121–122:57–64. https://doi.org/10.1016/j.apcatb.2012.03.027
27. Widjonarko NE (2016) Introduction to advanced x-ray diffraction techniques for polymeric thin films. Coatings 6:54
28. Kang W, Li R, Wei D, Xu S, Wei S, Li H (2015) CTAB-reduced synthesis of urchin-like Pt–Cu alloy nanostructures and catalysis study towards the methanol oxidation reaction. RSC Adv 5: 94210–94215. https://doi.org/10.1039/C5RA20464J
29. Wang G, Li W, Wu N, Huang B, Xiao L, Lu J, Zhuang L (2019) Unraveling the composition-activity relationship of PtRu binary alloy for hydrogen oxidation reaction in alkaline media. J Power Sources 412:282–286. https://doi.org/10.1016/j.jpowsour.2018.11.026
30. Wang S, Chen ZG, Cole I, Li Q (2015) Structural evolution of graphene quantum dots during thermal decomposition of citric acid

and the corresponding photoluminescence. Carbon N Y 82:304–313. https://doi.org/10.1016/j.carbon.2014.10.075
31. Tang MYH, Shum HC (2016) One-step immunoassay of C-reactive protein using droplet microfluidics. Lab Chip 16:4359–4365. https://doi.org/10.1039/C6LC01121G
32. Oh YK, Joung HA, Kim S, Kim M-G (2013) Vertical flow immunoassay (VFA) biosensor for a rapid one-step immunoassay. Lab Chip 13:768–772. https://doi.org/10.1039/C2LC41016H
33. Park J, Park JK (2017) Pressed region integrated 3D paper-based microfluidic device that enables vertical flow multistep assays for the detection of C-reactive protein based on programmed reagent loading. Sensors Actuators B Chem 246:1049–1055. https://doi.org/10.1016/j.snb.2017.02.150
34. Centi S, Bonel Sanmartin L, Tombelli S et al (2009) Detection of c reactive protein (CRP) in serum by an electrochemical aptamer-based sandwich assay. Electroanalysis 21:1309–1315. https://doi.org/10.1002/elan.200804560
35. Molinero-Fernández Á, Arruza L, López MÁ, Escarpa A (2020) On-the-fly rapid immunoassay for neonatal sepsis diagnosis: C-reactive protein accurate determination using magnetic graphene-based micromotors. Biosens Bioelectron 158:112156. https://doi.org/10.1016/j.bios.2020.112156
36. Zhang X, Hu R, Zhang K, Bai R, Li D, Yang Y (2016) An ultrasensitive label-free immunoassay for C-reactive protein detection in human serum based on electron transfer. Anal Methods 8:6202–6207. https://doi.org/10.1039/C6AY01464J
37. Bryan T, Luo X, Bueno PR, Davis JJ (2013) An optimised electrochemical biosensor for the label-free detection of C-reactive protein in blood. Biosens Bioelectron 39:94–98. https://doi.org/10.1016/j.bios.2012.06.051
38. Gupta RK, Periyakaruppan A, Meyyappan M, Koehne JE (2014) Label-free detection of C-reactive protein using a carbon nanofiber based biosensor. Biosens Bioelectron 59:112–119. https://doi.org/10.1016/j.bios.2014.03.027
39. Mishra SK, Sharma V, Kumar D, Rajesh (2014) Biofunctionalized gold nanoparticle-conducting polymer nanocomposite based bioelectrode for CRP detection. Appl Biochem Biotechnol 174:984–997. https://doi.org/10.1007/s12010-014-0984-1
40. Ma Y, Yang J, Yang T, Deng Y, Gu M, Wang M, Hu R, Yang Y (2020) Electrochemical detection of C-reactive protein using functionalized iridium nanoparticles/graphene oxide as a tag. RSC Adv 10:9723–9729. https://doi.org/10.1039/C9RA10386D
41. Vermeeren V, Grieten L, Vanden Bon N et al (2011) Impedimetric, diamond-based immmunosensor for the detection of C-reactive protein. Sensors Actuators B Chem 157:130–138. https://doi.org/10.1016/j.snb.2011.03.037
42. Hu J, Zhang ZL, Wen CY, Tang M, Wu LL, Liu C, Zhu L, Pang DW (2016) Sensitive and quantitative detection of C-reaction protein based on immunofluorescent nanospheres coupled with lateral flow test strip. Anal Chem 88:6577–6584. https://doi.org/10.1021/acs.analchem.6b01427
43. Liu TZ, Hu R, Zhang X, Zhang KL, Liu Y, Zhang XB, Bai RY, Li D, Yang YH (2016) Metal–organic framework nanomaterials as novel signal probes for electron transfer mediated ultrasensitive electrochemical immunoassay. Anal Chem 88:12516–12523. https://doi.org/10.1021/acs.analchem.6b04191
44. Lee SH, Choi S, Kwon K, Bae NH, Kwak BS, Cho WC, Lee SJ, Jung HI (2017) A photothermal biosensor for detection of C-reactive protein in human saliva. Sensors Actuators B Chem 246:471–476. https://doi.org/10.1016/j.snb.2017.01.188
45. Andersson PO, Viberg P, Forsberg P, Nikolajeff F, Österlund L, Karlsson M (2016) Nanocrystalline diamond sensor targeted for selective CRP detection: an ATR-FTIR spectroscopy study. Anal Bioanal Chem 408:3675–3680. https://doi.org/10.1007/s00216-016-9485-0
46. Xie J, Tang MQ, Chen J, Zhu YH, Lei CB, He HW, Xu XH (2020) A sandwich ELISA-like detection of C-reactive protein in blood by citicoline-bovine serum albumin conjugate and aptamer-functionalized gold nanoparticles nanozyme. Talanta 217:121070. https://doi.org/10.1016/j.talanta.2020.121070
47. Sloan-Dennison S, Laing S, Shand NC, Graham D, Faulds K (2017) A novel nanozyme assay utilising the catalytic activity of silver nanoparticles and SERRS. Analyst 142:2484–2490. https://doi.org/10.1039/C7AN00887B
48. Kim MS, Cho S, Joo SH, Lee J, Kwak SK, Kim MI, Lee J (2019) N- and B-codoped graphene: a strong candidate to replace natural peroxidase in sensitive and selective bioassays. ACS Nano 13:4312–4321. https://doi.org/10.1021/acsnano.8b09519